CRISPR-Cas12a-mediated label-free electrochemical aptamer-based sensor for SARS-CoV-2 antigen detection

Na Liu [a],[1], Ran Liu [a],[1], Jingjing Zhang [a],[b],[*]

[a] *State Key Laboratory of Analytical Chemistry for Life Science, School of Chemistry and Chemical Engineering, Nanjing University, Nanjing 210023, China*
[b] *Chemistry and Biomedicine Innovation Center (ChemBIC), Nanjing University, Nanjing 210023, China*

A B S T R A C T

Serological antigen testing has emerged as an important diagnostic paradigm in COVID-19, but often suffers from potential cross-reactivity. To address this limitation, we herein report a label-free electrochemical aptamer-based sensor for the detection of SARS-CoV-2 antigen by integrating aptamer-based specific recognition with CRISPR-Cas12a-mediated signal amplification. The sensing principle is based on the competitive binding of antigen and the preassembled Cas12a-crRNA complex to the antigen-specific aptamer, resulting in a change in the collateral cleavage activity of Cas12a. To further generate an electrochemical signal, a DNA architecture was fabricated by in situ rolling circle amplification on a gold electrode, which serves as a novel substrate for Cas12a. Upon Cas12a-based collateral DNA cleavage, the DNA architecture was degraded, leading to a significant decrease in impedance that can be measured spectroscopically. Using SARS-CoV-2 nucleocapsid antigen as the model, the proposed CRISPR-Cas12a-based electrochemical sensor (CRISPR-E) showed excellent analytical performance for the quantitative detection of nucleocapsid antigen. Since in vitro selection can obtain aptamers selective for many SARS-CoV-2 antigens, the proposed strategy can expand this powerful CRISPR-E system significantly for quantitative monitoring of a wide range of COVID-19 biomarkers.

1. Introduction

The COVID-19 pandemic has stimulated a growing demand for high-performance diagnostic tests, which are essential for the prevention, identification, and treatment of virus spread [1]. Currently, diagnosis for COVID-19 mainly relies on molecular tests, serological tests for antibodies and antigens, computed tomography (CT), and other clinical biomarkers of infected people [2,3]. While RT–qPCR-based nucleic acid detection is recommended as the gold standard, serological antigen testing has been recognized as an important complementary method to improve the accuracy of COVID-19 diagnosis [4]. For example, a recent study suggested that severe COVID-19 is associated with elevated serum N antigen (400–600 pg mL^{-1}) [5]. Despite the importance, rapid and accurate detection of SARS-CoV-2 antigens is still challenging due to their short diagnostic window, relatively low abundance and antibody cross-reactivity. Therefore, it is beneficial to develop improved

strategies for rapid, accurate and sensitive detection of SARS-CoV-2 antigens.

Recently, CRISPR-Cas has emerged as a powerful technology that is revolutionizing next-generation diagnostic platforms [6,7]. The mechanism of CRISPR-Cas systems, which are programmed by CRISPR guide RNA (crRNA), has been reported to not only cleave the target nucleic acid but also cleave all neighbouring nucleic acids indiscriminately [8,9]. This target-triggered collateral activity of CRISPR-Cas systems has stimulated the development of CRISPR-based biosensing technologies [10,11], which offer unique advantages of simple fabrication, ultrahigh sensitivity, high specificity to single-base variation, and good amenability for POC diagnostics [12–14]. On the basis of these advantages, CRISPR has been extensively used in designing biosensors for nucleic-acid-related COVID-19 diagnostics [15–19]. While promising in nucleic acid detection, to the best of our knowledge, few studies reported the use of CRISPR technology in the detection of SARS-CoV-2

---

  * Corresponding author.
    E-mail address: jing15209791@nju.edu.cn (J. Zhang).
  [1] *These authors contributed equally to this work.*

antigens [20]. Such limited attention is not consistent with the remarkable properties and potential merits of CRISPR.

A major challenge to develop CRISPR-based sensors for SARS-CoV-2 antigens lies in finding a method to link the antigen recognition event with the collateral cleavage activity of Cas effectors, which is typically activated by the specific binding of the crRNA to its target DNA/RNA [21]. To overcome this limitation, we have recently presented a proof-of-concept of a target-responsive CRISPR system by integrating an antibody-assisted proximity ligation assay with CRISPR technologies [21], and demonstrated its utility for detecting both nucleocapsid and spike (S) antigens. Although promising, it still requires multiple reagent manipulation steps and synthesis of antibody-DNA conjugates, which is time-consuming and labor-intensive. To explore new dimensions in CRISPR-based COVID-19 diagnostics, it would be of great interest to combine CRISPR–based sensors with new signal transduction strategies to create an intelligent sensing system for simple, cost-effective, label-free, and sensitive detection of SARS-CoV-2 antigens.

Electrochemical biosensors have been recognized as promising analytical techniques with burgeoning research attention during the COVID-19 pandemic, due to their unique superiorities of easy operation, cost effectiveness, rapid response, and high sensitivity [22–24]. In the past three years, several electrochemical biosensors have been developed for detecting SARS-CoV-2 antigens based on diverse modified electrodes [25–29]. Despite such successes, the majority of these strategies either require sophisticated fabrication of an electrochemically responsive interface or synthesis of electroactive labels that link to bioreceptors [30,31], or suffer from potential cross-reactivity of SARS-CoV-2 antibodies with antibodies generated against other coronaviruses due to their high genome similarities [32–35]. These drawbacks thereby result in potential tradeoffs in terms of sensitivity, specificity and user-friendliness. On the other hand, aptamers, known as "chemical antibodies", have been recommended as a powerful class of bioreceptors with several features of high specificity and affinity, reliable and cost-effective synthesis, ease of modification, and excellent feasibility to combine with many DNA-based reactions for signal amplification [36–38]. These advantages enable aptamers to be promising bioreceptors, with a wide range of applications for biosensors [39–47]. For example, Tang et al. developed a smart aptamer-gated mesoporous silica nanoplatform for visual fluorescence detection of carcinoembryonic antigen (CEA) [45]. Afterward, this group reported a series of elegant aptasensors for photoelectrochemical detection of CEA based on up-converting nanocrystals [46,47], with the merits of high sensitivity and selectivity. More recently, Luo et al. selected a specific aptamer targeting N protein of SARS-CoV-2 (N48) with high affinity (association rate constant of 8.80×10^5 M^{-1} s^{-1}) [48]. From this perspective, interfacing aptamers with CRISPR technologies for the construction of electrochemical aptasensors is expected to provide better biosensing performance toward precisely quantification of the SARS-CoV-2 antigen.

Herein, we present a label-free electrochemical aptasensing method for SARS-CoV-2 antigen detection by integrating aptamer-based specific recognition with CRISPR-Cas12a-mediated signal amplification. The sensor is based on the competitive binding of antigen and the preassembled Cas12a-crRNA complex to the antigen-specific aptamer, resulting in a change in the collateral cleavage activity of Cas12a. To realize the label-free electrochemical detection of antigens, a DNA architecture was fabricated by in situ rolling circle amplification (RCA) on a gold electrode, which serves as a novel substrate for Cas12a. Upon Cas12a-based collateral DNA cleavage, the DNA architecture was degraded, leading to a significant decrease in the electrochemical signal measured by electrochemical impedance spectroscopy (EIS). Such a construct combines key features of aptamers, RCA, and CRISPR technologies to improve specificity and sensitivity, followed by directly quantifying antigens using an EIS readout in a label-free format. Using nucleocapsid protein (N protein) as a model antigen, the proposed CRISPR–based electrochemical aptamer-based sensor (CRISPR-E) achieved a high sensitivity of 0.077 ng mL^{-1} for the N protein and high

specificity to accurately discriminate N protein from other coronaviruses. Although the CRISPR-E system was developed in the context of SARS-CoV-2 antigens, we anticipate that this new platform can be expanded to detect other protein biomarkers of COVID-19 through the use of suitable functional aptamers.

2. Experimental section

2.1. Materials and apparatus

All the materials and apparatuses are described in the electronic supplementary material (see S1 and S2).

2.2. Preparation of a circular DNA template

The circular DNA template (c-DNA) was synthesized by mixing 10 μL of Padlock DNA (pL-DNA, 10 μM), 10 μL of linker DNA (L-DNA, 10 μM), 10 μL of 10 × T4 DNA ligase buffer and 67.5 μL of Millipore water. After annealing at 90 °C for 5 min, the resulting solutions were slowly cooled to room temperature. After that, 2.5 μL of 40,000 units/mL T4 DNA ligase was added and incubated at 16 °C for 1 h to activate the ligation reaction. Finally, the obtained c-DNA product was separated and purified using denatured polyacrylamide gel electrophoresis (PAGE, 10%), suspended in Millipore water and ready to serve as the template for further rolling circle amplification.

2.3. Fabrication of the DNA-modified electrode through in-situ rolling circle amplification

First, a gold electrode was polished using 0.05 μm alumina slurry (Beuhler) followed by rinsing thoroughly with water. After successive sonication in ethanol and water, the electrode was scanned in 0.5 M H_2SO_4 between −0.2 and 1.6 V at 100 mV s^{-1} until a reproducible cyclic voltammogram was obtained. Before modification, thiolated primer DNA (SH-DNA) was activated with 10 mM TCEP in pH 7.4 Tris-HCl buffer for 2 h. Afterwards, 6 μL of 200 nM SH-DNA was spread on the precleaned Au electrode surface for 1 h at 37 °C in 100% humidity, followed by washing using PBS buffer to remove nonspecific adsorption. Subsequently, 6 μL of RCA solution consisting of c-DNA (0.2 μM), dNTPs (1 mM), and phi29 in 1 × phi29 DNA polymerase buffer was added onto the electrode surface to trigger the in situ RCA reaction. After incubating at 37 °C for 1 h, the obtained RCA-Au electrode was washed with PBS buffer, and used immediately for the following CRISPR-Cas12a assay.

2.4. Preparation of the CRISPR-based sensor and electrochemical/optical analysis

The CRISPR-based sensor for nucleocapsid antigen detection was based on the competitive binding of antigen and the preassembled Cas12a-crRNA complex to the antigen-specific aptamer. In a typical experiment, 2 μL of N48 aptamer (1.0 nM) was preincubated with 2 μL of different concentrations of nucleocapsid antigen for 20 min at 25 °C. Afterwards, 10 μL of preassembled Cas12a-crRNA complex (100 nM) was added and incubated for another 20 min to activate the collateral cleavage activity of Cas12a.

For electrochemical analysis, 6 μL of the above activated Cas12a solution was dropped onto the RCA-Au electrode surface, and reacted for 60 min. Finally, the electrode was washed thoroughly with pH 7.4 PBS buffer to remove nonspecifically bound biomolecules to minimize the background response. Electrochemical measurements including EIS and cyclic voltammetry (CV) were performed with a conventional three-electrode system as described in S1.2.

For optical analysis, 48 μL of the above activated Cas12a solution was mixed with 2 μL of 10 μM ssDNA fluorescence reporter (F-Q reporter), and incubated at 37 °C for 1 h. After that, the fluorescent signal of the resulting solution was measured using an F-320

spectrophotometer. The excitation wavelength was 488 nm, and the fluorescence spectra were collected from 500 nm to 650 nm. Control experiments either without crRNA or N48 were performed under the same conditions.

3. Results and discussion

3.1. Detection strategy and workflow of the aptamer-based electrochemical sensor for nucleocapsid antigen

Herein, we present the first report of integrating aptamer-based specific recognition of SARS-CoV-2 antigen with CRISPR-Cas12a-mediated signal amplification, and demonstrate a label-free platform for a CRISPR–based electrochemical sensor (CRISPR-E) responsive to the antigen. Our CRISPR-E system is mainly composed of three components (Scheme 1): competitive binding of antigen and the preassembled Cas12a-crRNA complex to the antigen-specific aptamer, which establishes the relationship between target antigen concentration and the collateral cleavage activity of Cas12a; a DNA RCA-Au electrode fabricated by in situ rolling circle amplification, which acts as the substrate of Cas12a for signal amplification; and an electrochemical workstation, which is used as a downstream transducer for electrochemical signal output. In the absence of the antigen target, the preassembled Cas12a-crRNA complex could recognize and hybridize with a fixed concentration of aptamer, thereby resulting in high collateral DNA cleavage activity of Cas12a. In contrast, in the presence of the antigen target, antigen and Cas12a-crRNA complex will compete for binding to the aptamer. As a result, less aptamer would be available to hybridize with the Cas12a-crRNA complex, leading to low collateral DNA cleavage activity of Cas12a. In this case, when the RCA-Au electrode was applied as the substrate of Cas12a, active Cas12a cleaved the RCA-DNA architecture, resulting in a decrease in electron-transfer resistance measured by electrochemical impedance spectroscopy (EIS). The EIS signal is directly related to the presence and integrity of the RCA-DNA architecture, which in turn depends on the collateral DNA cleavage activity of Cas12a that was regulated by target-induced competition. Consequently, the antigen target can be determined by monitoring the CRISPR-RCA-amplified EIS signal.

3.2. Feasibility of the aptamer-CRISPR-Cas12a assay for nucleocapsid antigen

To demonstrate the proof of principle, we first designed and synthesized a circular DNA template (c-DNA) based on the intramolecular ligation of padlock DNA (pL-DNA) in the presence of linker DNA (L-DNA) and T4 DNA ligase (Fig. S1A). The ligation process was confirmed by denatured polyacrylamide gel electrophoresis (PAGE). As shown in Fig. S1B, c-DNA displays a much slower were excess DNA electrophoretic mobility (lane 3) than the basic building units of L-DNA (lane 1) and linear pL-DNA (lane 2). This result illustrated the successful

accomplishment of intramolecular ligation. Afterwards, an RCA reaction was designed using c-DNA as the template and primer DNA (SH-DNA) as the trigger (Fig. 1A). The RCA process was further characterized by PAGE. As displayed in Fig. 1B, from lane 1 to lane 4, the bands indicate the individual SH-DNA, L-DNA, pL-DNA, and c-DNA, respectively. After the RCA reaction, a band with slower migration corresponding to the RCA product was observed (lane 5), indicating that SH-DNA could initiate the RCA reaction with the high-displacement activity of phi29 DNA polymerase for producing a long DNA architecture.

Next, we explored whether the antigen-specific aptamer could trigger the activation of Cas12a. To this aim, N protein, which is the most abundant and relatively conserved structural protein in SARS-CoV-2, was first chosen as a model antigen target, while the ssDNA aptamer (N48) was chosen as the recognition element [48]. As shown in Fig. 1B, when RCA-DNA was treated with a mixture solution of the N48 aptamer and the preassembled Cas12a-crRNA complex, multiple bright bands with lower molecular weights were observed (lane 6), indicating the enzymatic digestion of RCA products. In contrast, in the presence of N protein, fewer bands with slower migration were observed (lane 7). In addition, the presence of non-specific protein (spike S1) didn't produce significant difference referring to the bands compared to the control samples (lane 6). These results indicate the successful aptamer-triggered activation of Cas12a and the antigen-dependent inhibition of Cas12a. The morphology of the proposed CRISPR-RCA process initiated by the N48 aptamer was further investigated by atomic force microscopy (AFM). As expected, compared with the SH-DNA that displays some small spots (Fig. 1C), long and linear DNA nanowires were observed after the RCA reaction with a height of 1 nm (Fig. 1D). Moreover, treating the RCA-DNA architecture with active Cas12a results in linear but much shorter DNA nanowires with a height of 1 nm (Fig. 1E). Furthermore, introducing N protein to the above Cas12a-RCA reaction results in partially cutting of the DNA nanowires into small fragments (Fig. 1F). These results indicate that the N48 aptamer could trigger the CRISPR-RCA reaction with high efficiency that generates a significant amount of DNA fragments, while the introduction of N protein could partially inhibit the collateral DNA cleavage activity of Cas12a, which is consistent with the results obtained by PAGE (Fig. 1B).

Having demonstrated the successful CRISPR-RCA process, we then investigated the feasibility of our aptamer-CRISPR-Cas12a system for the detection of SARS-CoV-2 antigens. We first performed a fluorescence assay by introducing a 5 nt ssDNA reporter (TTATT) as the substrate for Cas12a–crRNA (Fig. 2A), with a fluorophore (FAM) and quencher (BHQ-1) conjugated at the 5′ and 3′ ends, respectively (denoted as ssDNA-FQ). As shown in Fig. 2B, in the absence of either aptamer or crRNA, a minimal fluorescence signal was observed when ssDNA-FQ was incubated with Cas12a–crRNA, while a considerable fluorescent signal was observed in the presence of 1 nM N48 aptamer. Furthermore, upon the addition of 25 ng mL^{-1} of N protein, a dramatic decrease in the fluorescent signal was obtained, and the fluorescence intensity further decreased with 100 ng mL^{-1} of N protein. These results were due to the
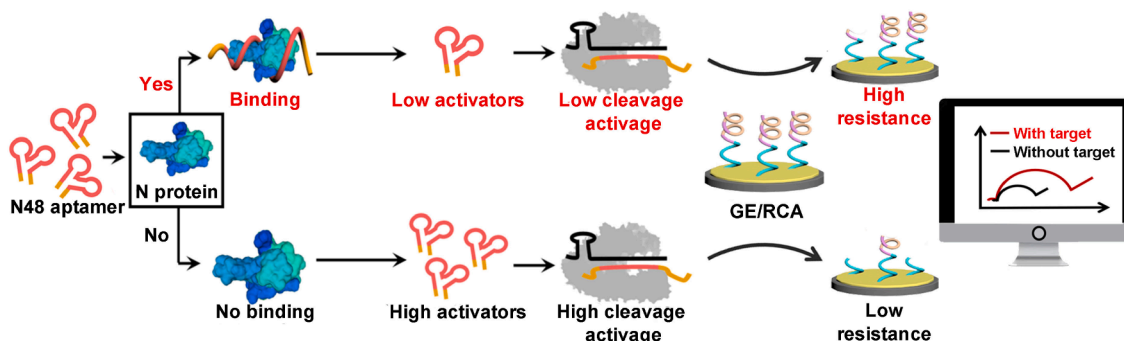
Scheme 1. Detection strategy and workflow of our CRISPR–based electrochemical sensor for SARS-CoV-2 antigen detection.
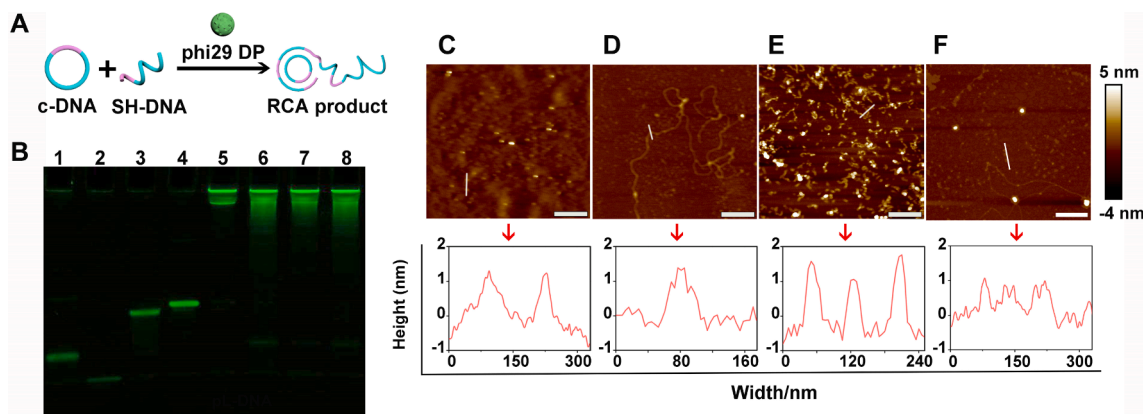
Fig. 1. Design and validation of the proposed CRISPR-RCA process. (A) Schematic illustration of the rolling-circle amplification (RCA) reaction. (B) Native PAGE (10%) characterization of the aptamer-regulated CRISPR-RCA process. AFM characterization of SH-DNA (C), RCA-DNA (D), and RCA-DNA treated with aptamer-activated Cas12a in the absence (E) and presence of 100 ng mL^{-1} N protein (F), with cross sectional profiles of the white lines in each panel.
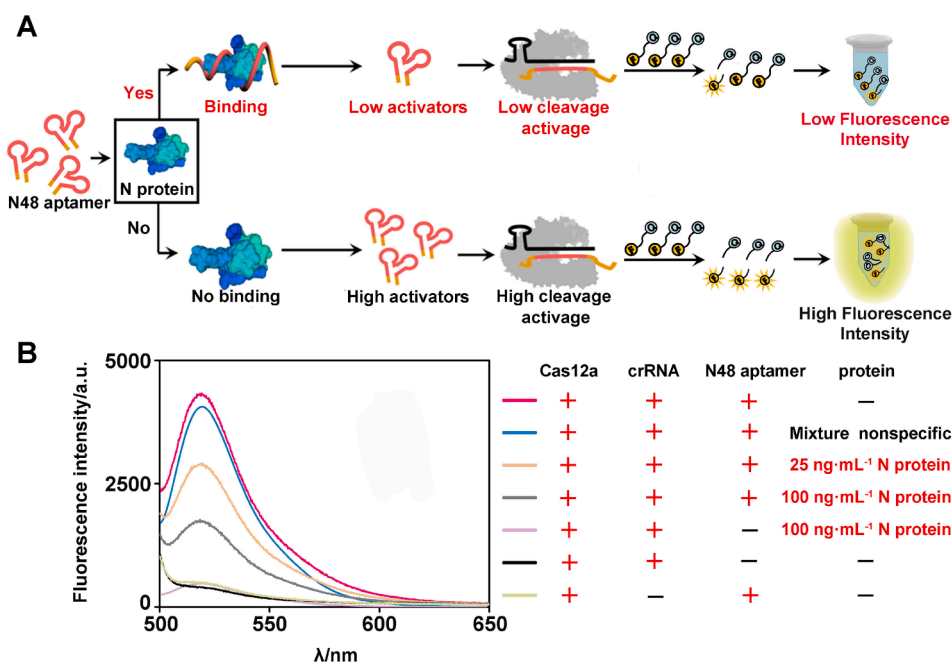

Fig. 2. Graphical illustration (A) and fluorescence monitoring (B) of the aptamer-regulated CRISPR-RCA system for the detection of SARS-CoV-2 antigens using a single-stranded DNA fluorescent reporter. The symbols "+" and "-", indicate the presence and absence of the corresponding molecules, respectively.

dose-dependent competitive binding of N protein and the preassembled Cas12a-crRNA complex to the N48 aptamer, resulting in the inhibition of collateral DNA cleavage activity of Cas12a. In addition, the non-specific protein (Spike S1) has a negligible effect to the fluorescence signal, compared with the control groups. Taken together, the above experimental results indicated the successful conversion of aptamer-based antigen recognition to the cleavage of RCA-DNA through the CRISPR-RCA process, forming the basis for subsequent electrochemical detection of the N protein.

3.3. Electrochemical characterization of the electrode

Encouraged by the above successful fluorescence assay for the N protein, we further developed a label-free CRISPR-based electro-chemical sensor (CRISPR-E) by introducing an RCA-DNA-modified electrode as the substrate for Cas12a–crRNA. The programmable assembly of the RCA-DNA architecture, as illustrated in Fig. S2 (the DNA sequences are shown in Table S1 in the ESI†), includes two steps. First,

thiolated primer DNA (SH-DNA) was immobilized on the gold electrode (GE) through Au-S bonds. Then, the aforementioned c-DNA was applied and served as the template to initiate the in situ RCA, producing a large amount of RCA-DNA product-immobilized on the gold electrode surface (RCA/GE). We first employed cyclic voltammetry to evaluate the successful assembly of these DNA-RCA products. As shown in Fig. 3A, compared with the bare gold electrode, the SH-DNA modified electrode exhibited a decrease in peak current but an increase in potential peak separation (ΔE_p). Additionally, ΔE_p further increased significantly for the RCA-DNA gold electrode (RCA/GE), indicating a much slower electron-transfer due to the large steric hindrance of the RCA-DNA architecture. Notably, when the RCA/GE was further treated with Cas12a RNP and N48 aptamer, an increase in peak current but a decrease in ΔE_p was observed, which was due to the disassembly of RCA-DNA architecture on the GE through collateral cleavage by Cas12a. Fig. 3B displays the CVs of the RCA-DNA gold electrode with varying scan rates from 0.04 to 0.25 V/s. The cathodic and anodic peak currents both increased with increasing scan rates, and the corresponding peak potentials
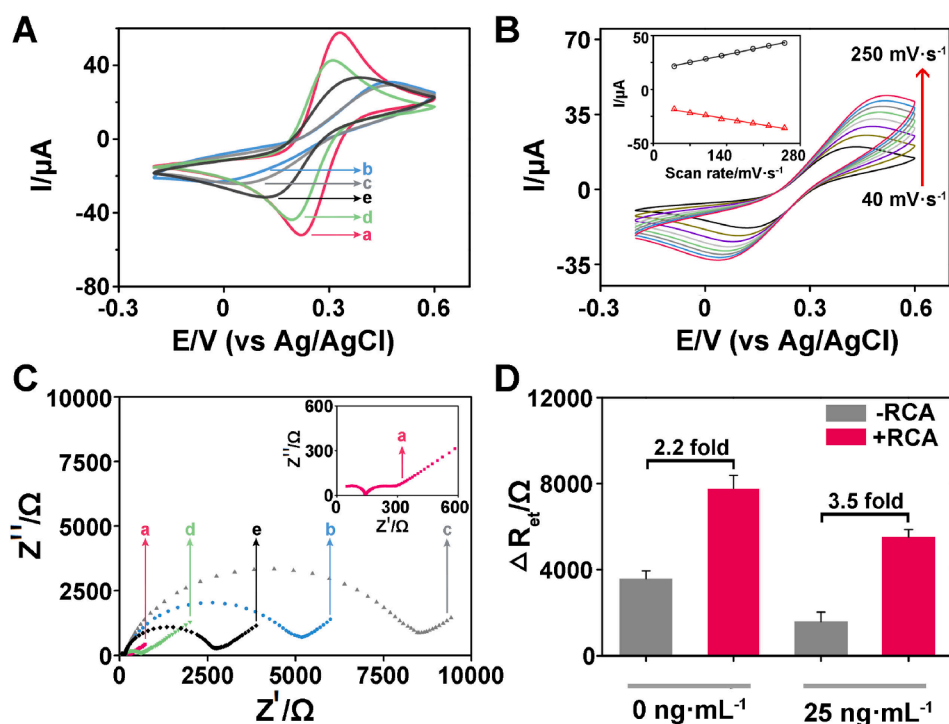
Fig. 3. Electrochemical characterization of the CRISPR-based electrochemical sensor. (A) CV responses of (a) bare gold electrode (GE), (b) SH-DNA/GE, (c) RCA/GE, RCA/GE with Cas12a RNP and aptamer in the absence (d) and presence (e) of N protein, respectively. (B) CVs of RCA-DNA gold electrode (RCA/GE) in 5 mM with different scan rates (40–250 mV s^{-1}). (C) Nyquist diagrams of electrochemical impedance spectra recorded from 0.01 to 10^6 Hz during the CRISPR-RCA process. Curves from a to e represent the same electrodes as CV measurements in Fig. 3A. (D) Comparison of EIS amplification capability for the detection of N protein by the CRISPR-E sensor with (+RCA) and without (−RCA) amplification. All electrochemical measurements were performed in 5 mM $[Fe(CN)_6]^{3-}/[Fe(CN)_6]^{4-}/$ 0.1 M KCl soultion. Error bars represent the standard deviations of three independent measurements.

showed a slight shift with an increase in the peak-to-peak separation. Moreover, both the cathodic and anodic peak currents increased linearly with scan rates from 0.04 to 0.25 V/s (Fig. 3B, inset) with a slope value of approximately 0.1, indicating a surface-controlled electrochemical process. Taken together, these results demonstrate the successful fabrication of DNA architecture on the electrode surface through the RCA process, forming the basis for the preparation of Cas12a-responsive substrates for subsequent electrochemical detection.

The fabrication process of the electrode was also characterized by electrochemical impedance spectroscopy (EIS) using $[Fe(CN)_6]^{3-/4-}$ as the redox probe. The semicircle at the higher-frequency range of the impedance spectra reveals an electron-transfer-limited process that could reflect the value of electron-transfer resistance (R_{et}). As shown in Fig. 3C, the bare gold electrode shows a very small semicircular domain (a), implying a relatively small R_{et}. With the immobilization of SH-DNA (b), the R_{et} increased because of the large steric hindrance of DNA. In addition, after the RCA reaction, the RCA gold electrode displays a significant increase in R_{et}, demonstrating the formation of an RCA-DNA architecture on the electrode. However, the R_{et} decreased dramatically after further incubation with the Cas12a-crRNA-aptamer complex, indicating the degradation of the RCA-DNA architecture due to collateral cleavage by aptamer-activated Cas12a. Finally, when the RCA-DNA-Au electrode was treated with the Cas12a-crRNA-aptamer complex in the presence of 50 pM N protein, a much smaller decrease in Ret was observed due to the competitive inhibition of Cas12a-crRNA with the N protein. These results were consistent with the fact that the CRISPR-E system was fabricated as expected.

To verify that the RCA-DNA architecture achieves a dramatically improved electrochemical signal compared with the small p-DNA, we compared the EIS response of the prepared CRISPR-E sensor to that of the sensor with the same concentration of N protein. As exhibited in Fig. 3D, when compared with the R_{et} change of the CRISPR-E sensor for 500 pM of N protein using SH-DNA-modified electrode as the substrate of Cas12a, the corresponding R_{et} change with the RCA-DNA gold electrode was approximately 3.5 times higher. These results suggest a good signal amplification capability of CRISPR-E because a small amount of the antigen target could be converted to a significant change in the collateral cleavage activity of Cas12a, achieving CRISPR-RCA-mediated signal amplification.

3.4. Analytical performance of the CRISPR-E sensor

To obtain the high performance of the CRISPR-E sensor, the effects of various experimental parameters, including the concentrations of Cas12a-crRNA complex and N48, RCA reaction time, and Cas12a cleavage time, were first investigated. Specifically, the concentrations of Cas12a-crRNA complex and N48 aptamer were optimized using a fluorescence assay. As shown in Fig. S3A and S3B, with increasing concentrations of Cas12a-crRNA complex or N48 aptamer, the normalized fluorescence signal increased in a dose-dependent manner. Considering the real application, the optimal concentration of Cas12a-crRNA complex and N48 aptamer was chosen as 50 nM and 1.0 nM, respectively. Moreover, we also varied the RCA reaction time from 30 to 120 min, followed by a typical Cas12a-based cleavage assay using EIS. As shown in Fig. S3C, the lowest R_{et} value was obtained for 60 min RCA reaction. Therefore, 60 min RCA reaction was chosen for the subsequent electrochemical experiments. Finally, to evaluate the Cas12a activity towards the RCA DNA, we further conducted a cleavage assay by incubating RCA/GE with activated Cas12a for different times, followed by the EIS measurement. As shown in Fig. S3D, R_{et} value of RCA/GE decreased in a time-dependent fashion and reached a plateau at 60 min. Therefore, 60 min was chosen as the optimized Cas12a cleavage time hereafter.

To determine whether the CRISPR-E sensor could detect N protein quantitatively, we first measured the EIS of different concentrations of N protein added to NEB buffer. As shown in Fig. 4A, the R_{et} value increased with increasing N protein concentrations from 0 to 125 ng mL^{-1}, showing an increasing diameter of the semicircle on the Nyquist diagram. In addition, a good linear relationship was observed between the R_{et} value and the logarithm of the N protein concentration in the range of 0.05 ng mL^{-1} to 125 ng mL^{-1} (Fig. 4B), and a limit of detection (LOD) of 0.077 ng mL^{-1} was obtained based on a $3\sigma_b$/slope, where σ_b is the standard deviation of three blank samples and the slope is obtained from R_{et}-C curve. Furthermore, to investigate the amplification factor of our CRISPR-E sensor, SH-DNA/GE was also applied as the substrate of Cas12a and measured using EIS. As shown in Fig. S4, a LOD of 1.2 ng
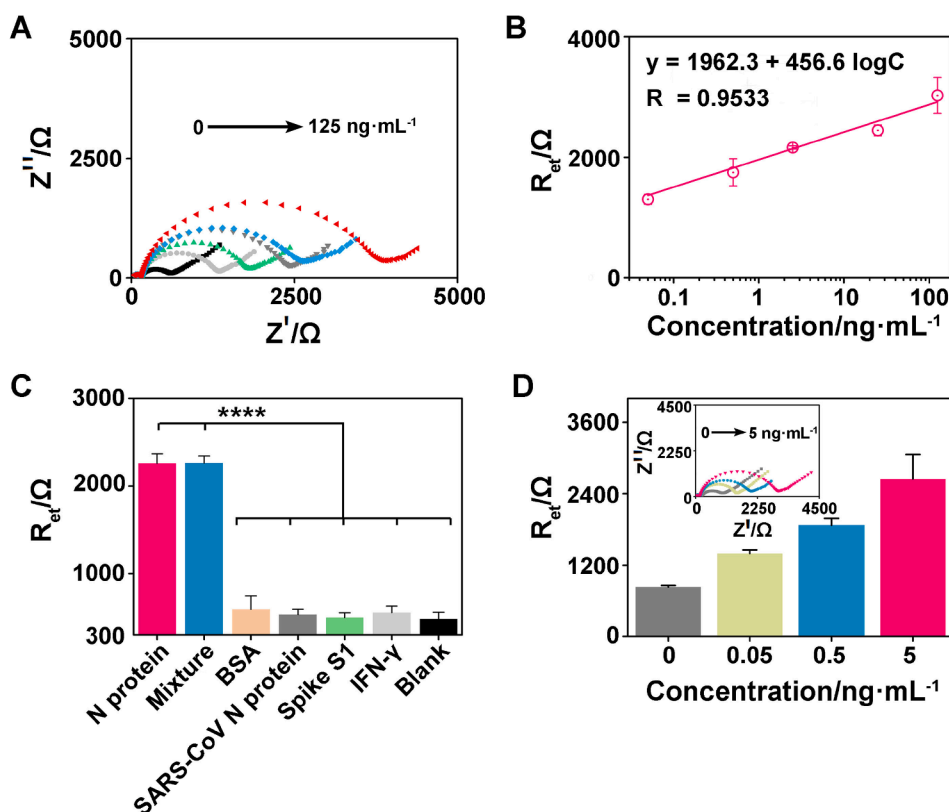
Fig. 4. Analytical performance of the CRISPR-E sensor. (A) Nyquist diagrams of EIS of the CRISPR-E sensor with different concentrations of N protein from 0.05 to 125 ng mL^{-1}. (B) Linear relationship between electron transfer resistance and logarithm of N protein concentration. Error bars represent the standard deviations of three independent measurements. (C) Selectivity of N protein detection. N protein: 0.5 ng mL^{-1}; BSA: 50 mg mL^{-1}; SARS-CoV N protein: 500 ng mL^{-1}; spike S1: 5.0 ng mL^{-1}; IFN-γ: 0.5 ng mL^{-1}. **** indicated P < 0.0001. Error bars represent the standard deviations of three independent measurements. (D) EIS signal of the CRISPR-E sensor in response to N protein. Inset: Nyquist diagrams of EIS of the CRISPR-E sensor with different concentrations of N protein spiked in serum.

mL^{-1} was obtained for CRISPR-E without RCA amplification, and the amplification factor is calculated to be about 15-fold. Of note, when compared with other analytical methods, as illustrated in Table S2, the developed CRISPR-E aptamer-based sensor exhibited a remarkably wider linear range and a significantly improved sensitivity and selectivity, which could be attributed to the advantages of integrating aptamer-based specific recognition with CRISPR-RCA-mediated signal amplification.

To demonstrate the selectivity of the CRISPR-E sensor, we performed a CRISPR-E assay using different competing proteins and the R_{et} value of EIS was recorded (Fig. 4C), including the N protein of SARS-CoV, spike S1, interferon-gamma (IFN-γ), bovine serum albumin (BSA), and a mixture of N protein with the above four competing proteins. Compared with competing proteins at the indicated concentrations related to their respective diagnostic criteria [49], the R_{et} value in response to N protein of SARS-CoV-2 showed a significant increase (p < 0.0001). However, there was a minimum change in R_{et} value for all the tested competing proteins compared with the blank sample. In addition, we mixed N protein with these competing proteins together as mix samples, then performed selectivity test again. As shown in Fig. 4C, these competing proteins had a minimum affect to the N protein sensing. Together, these results suggested that the good selectivity of the N48 aptamer was maintained for the CRISPR-E sensor, which was consistent with previous reports [48,50].

To confirm the reproducibility of the CRISPR-E sensor, the EIS responses of eight different CRISPR-E sensors with 0.5 ng mL^{-1}N protein prepared in the same batch were investigated. As displayed in Fig. S5, a relative standard deviation (RSD) of 7.8% was achieved, indicating good reproducibility. Moreover, the stability, which was critical to its practical application especially in the complicated biological samples, was evaluated using an RCA-DNA-modified gold electrode. The electrode was tested by EIS every day. When not in use, it was stored at 4 °C. The RCA-DNA-modified electrode retained ∼ 80% of its original EIS response after 10 days of storage (Fig. S6), indicating that the fabricated

RCA-DNA-modified electrode could serve as a stable substrate for the Cas12a-based sensor.

To assess the effectiveness of the proposed CRISPR-E sensor in practical applications, we first tested it in human serum. N protein spiked serum samples were prepared by diluting the N protein standard into undiluted human serum, and tested according to the typical CRISPR-E experiment (Section 2.4). As shown in Fig. 4D (inset), we observed an increasing diameter of the semicircle on the Nyquist diagram with increasing concentrations of N protein added. In addition, a dose-dependent R_{et} response to N protein in the range of 0.05–5.0 ng mL^{-1} was obtained (Fig. 4D). Moreover, a LOD of 0.16 ng mL^{-1} was calculated based on a $3\sigma_b$/slope, where σ_b is the standard deviation of three blank serum samples. Finally, to confirm the reliability of the CRISPR-E sensor, a recovery test with added N protein standards in serum samples was conducted. According to the calibration curve in Fig. 4D, the recovery rate of N protein from the serum samples was obtained. As shown in Table S3, the recovery rates were between 98.0 % and 105.0 %, which showed that the proposed method has no systematic error. For comparison, a reverse transcription-qPCR (RT-qPCR) experiment was further designed by using N gene as a model (Table S1). Three concentrations of N gene (0.05, 0.5, 5.0 ng mL^{-1}) spiked in serum samples were evaluated. Fig. S7A showed qPCR curves of different concentrations of N gene, and the obtained Ct value decreased with increasing N gene concentrations from 0 to 5.0 ng mL^{-1} (Fig. S7B), which was consistent with the recovery results obtained using CRISPR-E sensor (Table S3). Taken together, these results indicated that our CRISPR-E aptamer-based sensor could provide an accurate and reliable approach for analyzing real biological samples.

4. Conclusions

In summary, this work demonstrated a proof of principle for the first attempt to integrate the CRISPR technique with an aptamer-based electrochemical sensor for label-free and ultrasensitive detection of

SARS-CoV-2 antigens. By combing the advantages of aptamer-based specific recognition with CRISPR-Cas12a-mediated rolling circle amplification, the proposed CRISPR-E showed a wide linear range and low detection limit for the detection of N protein. Moreover, this method showed good selectivity, acceptable reproducibility and stability, and could be used for the detection of N protein in real samples. Since in vitro selection can obtain aptamers selective for many SARS-CoV-2 associated antigens, the method demonstrated could provide an effective avenue for the diagnosis of COVID-19.

Ethical approval

The authors state that all experiments were performed in compliance with the relevant laws and institutional guidelines. The human serum samples used in this study were approved by the institutional committee of Nanjing University.

Declaration of Competing Interest

The authors declare that they have no known competing financial interests or personal relationships that could have appeared to influence the work reported in this paper.

Acknowledgements

Appendix A. Supplementary material

Supplementary data to this article can be found online at https://doi.org/10.1016/j.bioelechem.2022.108105.

References

[1] F. Wu, S.u. Zhao, B. Yu, Y.-M. Chen, W. Wang, Z.-G. Song, Y.i. Hu, Z.-W. Tao, J.-H. Tian, Y.-Y. Pei, M.-L. Yuan, Y.-L. Zhang, F.-H. Dai, Y.i. Liu, Q.-M. Wang, J.-J. Zheng, L. Xu, E.C. Holmes, Y.-Z. Zhang, A new coronavirus associated with human respiratory disease in China, Nature 579 (7798) (2020) 265–269.

[2] B. Udugama, P. Kadhiresan, H.N. Kozlowski, A. Malekjahani, M. Osborne, V.Y. C. Li, H.M. Chen, S. Mubareka, J.B. Gubbay, W.C.W. Chan, Diagnosing COVID-19: the disease and tools for detection, ACS Nano 14 (4) (2020) 3822–3835.

[3] L.J. Carter, L.V. Garner, J.W. Smoot, Y. Li, Q. Zhou, C.J. Saveson, J.M. Sasso, A. C. Gregg, D.J. Soares, T.R. Beskid, S.R. Jervey, C. Liu, Assay techniques and test development for COVID-19 diagnosis, ACS Cent. Sci. 6 (5) (2020) 591–605.

[4] C.Y.P. Lee, R.T.P. Lin, L. Renia, L.F.P. Ng, Serological Approaches for COVID-19: Epidemiologic Perspective on Surveillance and Control, Front. Immunol. 11 (2020) 879.

[5] F. Perna, S. Bruzzaniti, E. Piemonte, V. Maddaloni, L. Atripaldi, S. Sale, A. Sanduzzi, C. Nicastro, N. Pepe, M. Bifulco, G. Matarese, M. Galgani, L. Atripaldi, Serum levels of SARS-CoV-2 nucleocapsid antigen associate with inflammatory status and disease severity in COVID-19 patients, Clin. Immunol. 226 (2021) 108720.

[6] Y. Tang, L.u. Gao, W. Feng, C. Guo, Q. Yang, F. Li, X.C. Le, The CRISPR-Cas toolbox for analytical and diagnostic assay development, Chem. Soc. Rev. 50 (21) (2021) 11844–11869.

[7] P.D.P. Swetha, J. Sonia, K. Sapna, K.S. Prasad, Towards CRISPR powered electrochemical sensing for smart diagnostics, Curr. Opin. Electrochem. 30 (2021) 100829.

[8] R.J. Zeng, W.J. Wang, M.M. Chen, Q. Wan, C.C. Wang, D. Knopp, D.P. Tang, CRISPR-Cas12a-driven MXene-PEDOT:PSS piezoresistive wireless biosensor, Nano Energy 82 (2021) 105711.

[9] H. Gong, Y. Wu, R. Zeng, Y. Zeng, X. Liu, D. Tang, CRISPR/Cas12a-mediated liposome-amplified strategy for the photoelectrochemical detection of nucleic acid, Chem. Commun. 57 (71) (2021) 8977–8980.

[10] Y. Dai, R.A. Somoza, L. Wang, J.F. Welter, Y. Li, A.I. Caplan, C.C. Liu, Exploring the trans-cleavage activity of CRISPR-Cas12a (cpf1) for the development of a universal electrochemical biosensor, Angew. Chem. Int. Ed. 58 (48) (2019) 17399–17405.

[11] W. Feng, A.M. Newbigging, J. Tao, Y.R. Cao, H.Y. Peng, C. Le, J.J. Wu, B. Pang, J. Li, D.L. Tyrrell, H.Q. Zhang, X.C. Le, CRISPR technology incorporating

[12] amplification strategies: molecular assays for nucleic acids, proteins, and small molecules, Chem. Sci. 12 (13) (2021) 4683–4698.

[12] W. Feng, H. Peng, J. Xu, Y. Liu, K. Pabbaraju, G. Tipples, M.A. Joyce, H.A. Saffran, D.L. Tyrrell, S. Babiuk, H. Zhang, X.C. Le, Integrating reverse transcription recombinase polymerase amplification with CRISPR technology for the one-tube assay of RNA, Anal. Chem. 93 (37) (2021) 12808–12816.

[13] W.W.W. Hsiao, T.N. Le, D.M. Pham, H.H. Ko, H.C. Chang, C.C. Lee, N. Sharma, C. K. Lee, W.H. Chiang, Recent advances in novel lateral flow technologies for detection of COVID-19, Biosensors-Basel 11 (9) (2021) 295.

[14] U. Ganbaatar, C.C. Liu, CRISPR-based COVID-19 testing: toward next-generation point-of-care diagnostics, Front. Cell. Infect. Microbiol. 11 (2021) 663949.

[15] J. Liu, Q. Wan, R. Zeng, D. Tang, An ultrasensitive homogeneous electrochemical biosensor based on CRISPR-Cas12a, Anal. Methods 13 (29) (2021) 3227–3232.

[16] Z. Huang, D. Tian, Y. Liu, Z. Lin, C.J. Lyon, W. Lai, D. Fusco, A. Drouin, X. Yin, T. Hu, B. Ning, Ultra-sensitive and high-throughput CRISPR-p owered COVID-19 diagnosis, Biosens. Bioelectron. 164 (2020) 112316.

[17] X. Ding, K. Yin, Z.Y. Li, R.V. Lalla, E. Ballesteros, M.M. Sfeir, C.C. Liu, Ultrasensitive and visual detection of SARS-CoV-2 using all-in-one dual CRISPR-Cas12a assay, Nat. Commun. 11 (1) (2020) 4711.

[18] H. Rahimi, M. Salehiabar, M. Barsbay, M. Ghaffarlou, T. Kavetskyy, A. Sharafi, S. Davaran, S.C. Chauhan, H. Danafar, S. Kaboli, H. Nosrati, M.M. Yallapu, J. Conde, CRISPR systems for COVID-19 diagnosis, ACS Sens. 6 (4) (2021) 1430–1445.

[19] R. Nouri, Z. Tang, M. Dong, T. Liu, A. Kshirsagar, W. Guan, CRISPR-based detection of SARS-CoV-2: a review from sample to result, Biosens. Bioelectron. 178 (2021) 113012.

[20] X. Zhao, Z. Wang, B. Yang, Z. Li, Y. Tong, Y. Bi, Z. Li, X. Xia, X. Chen, L. Zhang, W. Wang, G.-Y. Tan, Integrating PCR-free amplification and synergistic sensing for ultrasensitive and rapid CRISPR/Cas12a-based SARS-CoV-2 antigen detection, Synth. Syst. Biotechnol. 6 (4) (2021) 283–291.

[21] R. Liu, L. He, Y. Hu, Z. Luo, J. Zhang, A serological aptamer-assisted proximity ligation assay for COVID-19 diagnosis and seeking neutralizing aptamers, Chem. Sci. 11 (44) (2020) 12157–12164.

[22] L. Shi, L. Wang, X. Ma, X. Fang, L. Xiang, Y. Yi, J. Li, Z. Luo, G. Li, Aptamer-functionalized nanochannels for one-step detection of SARS-CoV-2 in samples from COVID-19 patients, Anal. Chem. 93 (49) (2021) 16646–16654.

[23] N. Kumar, N.P. Shetti, S. Jagannath, T.M. Aminabhavi, Electrochemical sensors for the detection of SARS-CoV-2 virus, Chem. Eng. J 430 (2022) 132966.

[24] R. Peng, Y. Pan, Z. Li, Z. Qin, J.M. Rini, X. Liu, SPEEDS: a portable serological testing platform for rapid electrochemical detection of SARS-CoV-2 antibodies, Biosens. Bioelectron. 197 (2022) 113762.

[25] R.M. Torrente-Rodriguez, H. Lukas, J.B. Tu, J.H. Min, Y.R. Yang, C.H. Xu, H. B. Rossiter, W. Gao, SARS-CoV-2 RapidPlex: a graphene-based multiplexed telemedicine platform for rapid and low-cost COVID-19 diagnosis and monitoring, Matter 3 (6) (2020) 1981–1998.

[26] A. Yakoh, U. Pimpitak, S. Rengpipat, N. Hirankarn, O. Chailapakul, S. Chaiyo, Paper-based electrochemical biosensor for diagnosing COVID-19: detection of SARS-CoV-2 antibodies and antigen, Biosens. Bioelectron. 176 (2021) 112912.

[27] A. Raziq, A. Kidakova, R. Boroznjak, J. Reut, A. Opik, V. Syritski, Development of a portable MIP-based electrochemical sensor for detection of SARS-CoV-2 antigen, Biosens. Bioelectron. 178 (2021) 113029.

[28] T. Beduk, D. Beduk, J.I. de Oliveira Filho, F. Zihnioglu, C. Cicek, R. Sertoz, B. Arda, T. Goksel, K. Turhan, K.N. Salama, S. Timur, Rapid point-of-care COVID-19 diagnosis with a gold-nanoarchitecture-assisted laser-scribed graphene biosensor, Anal. Chem. 93 (24) (2021) 8585–8594.

[29] V.J. Vezza, A. Butterworth, P. Lasserre, E.O. Blair, A. MacDonald, S. Hannah, C. Rinaldi, P.A. Hoskisson, A.C. Ward, A. Longmuir, S. Setford, E.C.W. Farmer, M. E. Murphy, D.K. Corrigan, An electrochemical SARS-CoV-2 biosensor inspired by glucose test strip manufacturing processes, Chem. Commun. 57 (30) (2021) 3704–3707.

[30] J. Munoz, M. Pumera, 3D-Printed COVID-19 immunosensors with electronic readout, Chem. Eng. J. 425 (2021) 131433.

[31] M.A. Zamzami, G. Rabbani, A. Ahmad, A.A. Basalah, W.H. Al-Sabban, S.N. Ahn, H. Choudhry, Carbon nanotube field-effect transistor (CNT-FET)-based biosensor for rapid detection of SARS-CoV-2 (COVID-19) surface spike protein S1, Bioelectrochemistry 143 (2022) 107982.

[32] C. Karaman, B.B. Yola, O. Karaman, N. Atar, I. Polat, M.L. Yola, Sensitive sandwich-type electrochemical SARS-CoV-2 nucleocapsid protein immunosensor, Microchim. Acta 188 (12) (2021) 425.

[33] G.C. Zaccariotto, M.K.L. Silva, G.S. Rocha, I. Cesarino, A novel method for the detection of SARS-CoV-2 based on graphene-impedimetric immunosensor, Materials 14 (15) (2021) 4230.

[34] M.A. Ali, C. Hu, S. Jahan, B. Yuan, M.S. Saleh, E. Ju, S.-J. Gao, R. Panat, Sensing of COVID-19 antibodies in seconds via aerosol jet nanoprinted reduced-graphene-oxide-coated 3D electrodes, Adv. Mater. 33 (7) (2021) 2006647.

[35] J. Li, P.B. Lillehoj, Microfluidic magneto immunosensor for rapid, high sensitivity measurements of SARS-CoV-2 nucleocapsid protein in serum, ACS Sens. 6 (3) (2021) 1270–1278.

[36] H. Yu, Z. Chen, Y. Liu, O. Alkhamis, Z. Song, Y.i. Xiao, Fabrication of aptamer-modified paper electrochemical devices for on-site biosensing, Angew. Chem. Int. Ed. 60 (6) (2021) 2993–3000.

[37] Z. Zhang, R. Pandey, J. Li, J. Gu, D. White, H.D. Stacey, J.C. Ang, C.-J. Steinberg, A. Capretta, C.D.M. Filipe, K. Mossman, C. Balion, M.S. Miller, B.J. Salena, D. Yamamura, L. Soleymani, J.D. Brennan, Y. Li, High-affinity dimeric aptamers enable the rapid electrochemical detection of wild-type and B.1.1.7 SARS-CoV-2 in unprocessed saliva, Angew. Chem. Int. Ed. 60 (45) (2021) 24266–24274.

[38] M. Mandal, N. Dutta, G. Dutta, Aptamer-based biosensors and their implications in COVID-19 diagnosis, Anal. Methods 13 (45) (2021) 5400–5417.

[39] X.N. Mi, H. Li, R. Tan, B.N. Feng, Y.F. Tu, The TDs/aptamer cTnI biosensors based on HCR and Au/Ti3C2-MXene amplification for screening serious patient in COVID-19 pandemic, Biosens. Bioelectron. 192 (2021) 113482.

[40] Z.W. Jiang, T.T. Zhao, C.M. Li, Y.F. Li, C.Z. Huang, 2D MOF-based photoelectrochemical aptasensor for SARS-CoV-2 spike glycoprotein detection, ACS Appl. Mater. Interfaces 13 (42) (2021) 49754–49761.

[41] A. Idili, C. Parolo, R. Alvarez-Diduk, A. Merkoçi, Rapid and efficient detection of the SARS-CoV-2 spike protein using an electrochemical aptamer-based sensor, ACS Sens. 6 (8) (2021) 3093–3101.

[42] J.J. Tian, Z.X. Liang, O. Hu, Q.D. He, D.P. Sun, Z.A.G. Chen, An electrochemical dual-aptamer biosensor based on metal-organic frameworks MIL-53 decorated with Au@Pt nanoparticles and enzymes for detection of COVID-19 nucleocapsid protein, Electrochim. Acta 387 (2021) 138553.

[43] S. Ramanathan, S.C.B. Gopinath, Z.H. Ismail, M.K.M. Arshad, P. Poopalan, Aptasensing nucleocapsid protein on nanodiamond assembled gold interdigitated electrodes for impedimetric SARS-CoV-2 infectious disease assessment, Biosens. Bioelectron. 197 (2022) 113735.

[44] J.C. Abrego-Martinez, M. Jafari, S. Chergui, C. Pavel, D.P. Che, M. Siaj, Aptamer-based electrochemical biosensor for rapid detection of SARS-CoV-2: Nanoscale electrode-aptamer-SARS-CoV-2 imaging by photo-induced force microscopy, Biosens. Bioelectron. 195 (2022) 113595.

[45] Z. Qiu, J. Shu, D. Tang, Bioresponsive release system for visual fluorescence detection of carcinoembryonic antigen from mesoporous silica nanocontainers mediated optical color on quantum dot-enzyme-impregnated paper, Anal. Chem. 89 (9) (2017) 5152–5160.

[46] Z. Qiu, J. Shu, J. Liu, D. Tang, Dual-channel photoelectrochemical ratiometric aptasensor with up-converting nanocrystals using spatial-resolved technique on homemade 3D printed device, Anal. Chem. 91 (2) (2019) 1260–1268.

[47] S.Z. Lv, K.Y. Zhang, L. Zhu, D.P. Tang, ZIF-8-assisted NaYF4:Yb, Tm@ZnO converter with exonuclease III-powered DNA walker for near-infrared light responsive biosensor, Anal. Chem. 92 (1) (2020) 1470–1476.

[48] L. Zhang, X. Fang, X. Liu, H. Ou, H. Zhang, J. Wang, Q. Li, H. Cheng, W. Zhang, Z. Luo, Discovery of sandwich type COVID-19 nucleocapsid protein DNA aptamers, Chem. Commun. 56 (70) (2020) 10235–10238.

[49] A.F. Ogata, A.M. Maley, C. Wu, T. Gilboa, M. Norman, R. Lazarovits, C.P. Mao, G. Newton, M. Chang, K. Nguyen, M. Kamkaew, Q. Zhu, T.E. Gibson, E.T. Ryan, R. C. Charles, W.A. Marasco, D.R. Walt, Ultra-sensitive serial profiling of SARS-CoV-2 antigens and antibodies in plasma to understand disease progression in COVID-19 patients with severe disease, Clin. Chem. 66 (12) (2020) 1562–1572.

[50] C. Han, W. Li, Q. Li, W. Xing, H. Luo, H. Ji, X. Fang, Z. Luo, L. Zhang, CRISPR/Cas12a-derived electrochemical aptasensor for ultrasensitive detection of COVID-19 nucleocapsid protein, Biosens. Bioelectron. 200 (2022) 113922.